Null-Space-Based Time-Varying Formation Control of Uncertain Nonlinear Second-Order Multiagent Systems With Collision Avoidance

Chang-Bing Zheng, Zhong-Hua Pang, *Senior Member, IEEE*, Jing-Xu Wang, Jian Sun, *Senior Member, IEEE*, Guo-Ping Liu, *Fellow, IEEE*, and Qing-Long Han, *Fellow, IEEE*

***Abstract*—In this article, the time-varying formation control problem with collision avoidance is addressed for uncertain nonlinear second-order multiagent systems in a null-space-based behavioral control architecture. To guarantee the tracking and coordination performance simultaneously, a novel and flexible time-varying formation task strategy is designed where only neighborhood information is necessary. Moreover, the agent radius and a sine function are introduced such that the collision avoidance task function describes collision risk more accurately in contrast to existing results. Then, two fixed-time sliding mode controllers with constant and variable exponent coefficients, respectively, are proposed to track the desired trajectory generated by null space projection. Also, the theoretical results for the task design and trajectory tracking are obtained by using the Lyapunov stability theory. Numerical simulation and practical experiments are finally conducted to illustrate the effectiveness and superiority of the proposed method.**

***Index Terms*—Collision avoidance (CA), fixed-time control, multiagent systems (MASs), null-space-based behavioral (NSB) control, sliding mode controller, time-varying formation.**

Manuscript received 9 June 2022; revised 2 September 2022 and 25 September 2022; accepted 20 October 2022. Date of publication 2 November 2022; date of current version 17 April 2023. This work was supported in part by the National Natural Science Foundation of China under Grant 62173002, Grant 61925303, Grant 62088101, Grant U20B2073, Grant 61720106011, and Grant 62173255, and in part by the Beijing Natural Science Foundation under Grant 4222045. *(Corresponding author: Zhong-Hua Pang.)*

Chang-Bing Zheng, Zhong-Hua Pang, and Jing-Xu Wang are with the Key Laboratory of Fieldbus Technology and Automation of Beijing, North China University of Technology, Beijing 100144, China (e-mail: cbzheng@mail.ncut.edu.cn; zhonghua.pang@ia.ac.cn; jxwangncut@mail.ncut.edu.cn).

Jian Sun is with the State Key Laboratory of Intelligent Control and Decision of Complex Systems, School of Automation, Beijing Institute of Technology, Beijing 100081, China, and also with the Beijing Institute of Technology Chongqing Innovation Center, Chongqing 401120, China (e-mail: sunjian@bit.edu.cn).

Guo-Ping Liu is with the Center for Control Science and Technology, Southern University of Science and Technology, Shenzhen 518055, China (e-mail: liugp@sustech.edu.cn).

Qing-Long Han is with the School of Science, Computing and Engineering Technologies, Swinburne University of Technology, Melbourne, VIC 3122, Australia (e-mail: qhan@swin.edu.au).

Color versions of one or more figures in this article are available at https://doi.org/10.1109/TIE.2022.3217585.

Digital Object Identifier 10.1109/TIE.2022.3217585

I. Introduction

TIME-VARYING formation of multiagent systems (MASs) is a significant topic and has attracted extensive attention, which has wider applications, e.g., resource exploration and collaborative rescue, compared with fixed formation. For second-order and higher-order MASs, the state or output time-varying formation problems were studied in [1], [2], [3], [4]. However, collision avoidance (CA) was not considered, which is essential due to unreasonable path planning and other stochastic factors. The collision between agents usually brings unrecoverable physical damage to the overall system, and thus, it is necessary for MASs to be equipped with the function of CA.

To deal with the collision problem, there are generally three categories of approaches, including model predictive control (MPC) approach, artificial potential field (APF) approach, and null-space-based behavioral (NSB) control approach. The MPC approach solves the optimization problem by considering distance or relative velocity constraints, and then generates a collision-free trajectory to achieve CA [5], [6], [7]. However, the high computational amount of the MPC approach is still a problem for distributed MASs with limited resources. The APF approach is that when an agent enters the potential field of another agent, it will be subject to a repulsive force so as to increase the distance between them [8], [9], [10]. Different from the APF approach, the NSB approach has the foresight ability for collision, and further is widely suggested in view of its capability to handle multitask constraints. The NSB approach was applied to multirobot systems in [11] as well as autonomous surface vessels in [12]. Later, in [13], the rigorous stability analysis was given, and a simple condition to ensure the validity of tasks was obtained. In [14], theoretical and experimental results were provided for the trajectory tracking of UAVs. In [15], the controller for spacecraft formation with CA was designed by combining the relative position control and NSB control scheme. By using a barrier Lyapunov function, in [16], state constraints were relaxed to be time-varying, while achieving spacecraft formation with obstacle/CA.

Note that the results of NSB control in [11], [12], [13], [14], [15], and [16] were only concerned with asymptotic stability. However, in practical MASs especially for time-varying formation, fast convergence is usually desired. Therefore, how to achieve time-varying formation in finite time is worth studying.

For second-order uncertain nonlinear MASs and multiple mechanical systems, finite-time fixed formation problems were investigated in [17], [18], [19]. Nevertheless, the convergence time is dominated by initial states, and the convergence rate would not be ideal with inappropriate initial states. Hence, fixed-time convergence was discussed for second-order nonlinear agents in [20]. In existing finite-time and fixed-time control results, however, formation tasks were designed simply to track the leader without considering coordination with neighbors, and only the fixed formation was considered. Accordingly, the first challenging issue to be addressed in this article is: How to design a flexible formation task strategy to achieve the time-varying formation? Furthermore, the distances between agents were not directly used to obtain desired velocities for CA such that collision risk could not be accurately described. Therefore, the second challenge is: How to design a novel and practical CA task function such that the desired velocities for CA are directly determined by the distances between agents?

In particular, sliding mode control is a remarkable strategy to solve the fixed-time convergence problem [21]. In [22], a time-independent controller using terminal sliding surface was designed to achieve fixed-time stability. In [23], the extension of constant upper bounds to time-varying upper functions, as well as fixed-time stability, was achieved by developing a variable-gain sliding mode controller. Then, a state-dependent variable exponent coefficient was introduced for fixed-time stability in [24], and the singularity problem could be eliminated. However, the results in [24] were limited to scalar systems, and also, only the stability problem of individual systems was discussed. Clearly, the third challenge to be handled lies in how to transform the tracking control problem into a stability problem, and theoretical analysis in multidimensional space needs to be performed. Moreover, to the best of our knowledge, very few results have considered time-varying formation with fixed-time tracking in an NSB architecture.

Motivated by the abovementioned observations, the fixed-time time-varying formation control problem with CA is investigated in this article for uncertain nonlinear second-order MASs using the NSB approach, and the main contributions corresponding to the aforementioned three challenges are summarized as follows.

1) *Design of the formation task:* Compared with [15], [16], [17], [18], [19], and [20], a novel and flexible time-varying formation task strategy is designed, where the coordination performance and tracking performance can be adjusted according to the needs of designers, such that the total coordination error can be significantly reduced.
2) *Design of the CA task:* In order to describe collision risk more accurately and expand application scenarios, a CA task function is presented by introducing the agent radius and a sine function, of which the desired velocity increases as the distance between agents decreases. Moreover, it is worthwhile to point out that the proposed method is innovative and different from the existing CA results in, e.g., [15], [16], [17], [18], [19], and [20].
3) *Design of the trajectory tracking algorithm:* By extending the results in [24] to the case of MASs in multidimensional space as well as integrating the sliding mode control and the NSB control, a robust fixed-time time-varying formation tracking control scheme is proposed, and the fixed-time results related to the number of agents are obtained.

The rest of this article is organized as follows. In Section II, the system description and preliminary are given. In Section III, the main results are presented for the desired trajectory generation and controller design of fixed-time trajectory tracking. Simulation and experimental results are provided in Section IV to demonstrate the validity of the proposed method. Finally, Section V concludes this article.

Notations: In this article, the superscript "T" denotes transposition. $\mathbb{R}^n$ is the n-dimensional Euclidean space. $\|\cdot\|_p$ is the p-norm. $\mathrm{sign}(\cdot)$ represents the sign function. The symbol (t) is omitted for simplicity throughout this article, e.g., $p_i(t)$ is simplified as p_i. The subscripts "i" and "j" of symbols correspond to agents i and j, respectively, which are used to denote two different agents.

II. System Description and Preliminary

A. System Description

In this article, a class of uncertain nonlinear second-order MASs with one virtual leader and N followers is considered. The virtual leader is labeled as $i = 0$, and the followers are $i = 1, 2, \ldots, N$. Their dynamics are described by

$$\begin{cases} \dot{p}_0 = v_0 \\ \dot{v}_0 = u_0 \end{cases} \tag{1}$$

$$\begin{cases} \dot{p}_i = v_i \\ \dot{v}_i = f(x_i) + g(x_i)u_i + d_i,\ i = 1, \ldots, N \end{cases} \tag{2}$$

where $x_i = [p_i^{\mathrm{T}},\ v_i^{\mathrm{T}}]^{\mathrm{T}} \in \mathbb{R}^6$, $p_i \in \mathbb{R}^3$, $v_i \in \mathbb{R}^3$, and $u_i \in \mathbb{R}^3$ are the state, position, velocity, and control input for agent i, $i = 0, 1, \ldots, N$, respectively, $f(\cdot)$ and $g(\cdot)$ are continuous nonlinear functions satisfying $f(0) = 0$ and $g(\cdot) \neq 0$, and $d_i \in \mathbb{R}^3$ is the parameteric uncertainty or external disturbance of follower i with $\|d_i\|_1 \leq \delta_1$, where $\delta_1 > 0$ is a constant.

B. Preliminary

A directed communication topology $\mathcal{G}$ without self-loops for followers is considered, and the adjacency matrix $\mathcal{A}$ is composed of element a_{ij}, where $a_{ij} = 1$ denotes agent i can receive information from agent j; otherwise $a_{ij} = 0$. To characterize the connections between followers and the virtual leader, the graph $\tilde{\mathcal{G}}$, including the graph $\mathcal{G}$ and the virtual leader, is introduced, in which the virtual leader is the root node. Let $b_i = 1$ when there is a directed path from the virtual leader to follower i; otherwise $b_i = 0$. It is essential that the graph $\tilde{\mathcal{G}}$ has a directed spanning tree.

Lemma 1 ([24] and [25]): Given the following nonlinear system:

$$\dot{z}(t) = h\left(z(t)\right),\ z(0) = z_0,\ z(t) \in \mathbb{R}^n \tag{3}$$

where $h(\cdot)$ is a continuous nonlinear function with $h(0) = 0$. If there exists a continuously differentiable positive definite

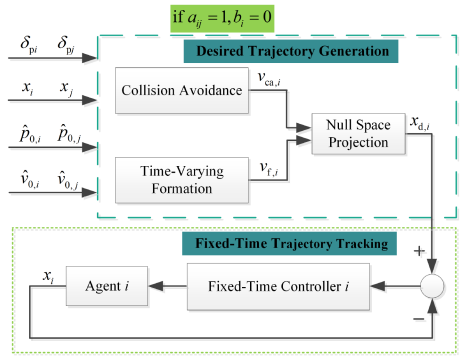

Fig. 1. Diagram of the proposed NSB control scheme.

Lyapunov function candidate $V(z)$ such that

$$\dot{V}(z) \le -\alpha_0 V^p(z) - \beta_0 V^q(z) \tag{4}$$

where $\alpha_0 > 0$, $\beta_0 > 0$, $p > 1$, and $0 < q < 1$ are all real numbers. Then, system (3) is fixed-time stable, and the settling time T is given by

$$T \le T_{\max} := \frac{1}{\alpha_0(p-1)} + \frac{1}{\beta_0(1-q)}. \tag{5}$$

Lemma 2 ([26]): For any $y_1, y_2, \ldots, y_n \ge 0$, the following inequalities hold:

$$\left(\sum_{i=1}^{n} y_i\right)^{\varsigma} \le \sum_{i=1}^{n} y_i^{\varsigma}, \text{ if } 0 < \varsigma \le 1 \tag{6}$$

$$n^{1-\varsigma}\left(\sum_{i=1}^{n} y_i\right)^{\varsigma} \le \sum_{i=1}^{n} y_i^{\varsigma}, \text{ if } \varsigma > 1. \tag{7}$$

Assumption 1: The control input u_0 (the acceleration of the virtual leader) is bounded.

III. Main Results

In this section, the generation of the desired dynamic path is presented by considering time-varying formation and CA simultaneously. After the desired trajectory is obtained, two fixed-time sliding mode controllers are designed by using constant and variable exponent coefficients, of which the theoretical analysis is given.

A. Desired Trajectory Generation

As shown in Fig. 1, the NSB control method is employed to perform both the time-varying formation task and the CA task. Clearly, the priority of the CA task is higher than that of the time-varying formation task. When the two tasks conflict with each other, the desired velocity of the low-priority task is projected onto the null space of the one of high-priority task, and thus, the desired state $x_{\mathrm{d},i}$, including the desired trajectory $p_{\mathrm{d},i}$ and the desired velocity $v_{\mathrm{d},i}$, can be obtained [19].

Define the time-varying formation task function as follows:

$$\sigma_{\mathrm{f},i} = p_i. \tag{8}$$

With the characteristic of time-varying formation, the coordinate of follower i in the desired time-varying formation is

$$\sigma_{\mathrm{fd},i} = \frac{\varrho_1(\hat{p}_{0,i} + \delta_{\mathrm{p}i}) + \varrho_2 \sum_{j=1}^{N} a_{ij}(p_j - \delta_{\mathrm{p}j} + \delta_{\mathrm{p}i})}{\varrho_1 + \varrho_2 \sum_{j=1}^{N} a_{ij}} \tag{9}$$

where the parameters $0 \le \varrho_1 \le 1$ and $0 \le \varrho_2 \le 1$ are used to adjust the weight of the tracking performance and the coordination performance with $\varrho_1 + \varrho_2 = 1$, respectively, $\delta_{\mathrm{p}i}$ is the desired position offset relative to the virtual leader and its derivative is bounded (clearly, the desired formation shape is determined by $\delta_{\mathrm{p}} = [\delta_{\mathrm{p}1}^{\mathrm{T}}, \delta_{\mathrm{p}2}^{\mathrm{T}}, \ldots, \delta_{\mathrm{p}N}^{\mathrm{T}}]^{\mathrm{T}}$), and $\hat{p}_{0,i}$ is the position estimate of the virtual leader in follower i, which can be obtained in finite time using the sliding mode estimator in [27] under Assumption 1 as follows:

$$\begin{cases} \dot{\hat{p}}_{0,i} = \hat{v}_{0,i} - c_1 \mathrm{sign}(\sum_{j=1}^{N} a_{ij}(\hat{p}_{0,i} - \hat{p}_{0,j}) \\ \quad + b_i(\hat{p}_{0,i} - p_0)) \\ \dot{\hat{v}}_{0,i} = -c_2 \mathrm{sign}(\sum_{j=1}^{N} a_{ij}(\hat{v}_{0,i} - \hat{v}_{0,j}) \\ \quad + b_i(\hat{v}_{0,i} - v_0)) \end{cases} \tag{10}$$

where c_1 and c_2 are the parameters of the estimator, and $\hat{v}_{0,i}$ is the velocity estimate of the virtual leader in follower i. Based on the NSB control method in [13], the desired velocity for time-varying formation is given as follows:

$$v_{\mathrm{f},i} = J_{\mathrm{f},i}^{\dagger}(\dot{\sigma}_{\mathrm{fd},i} + \lambda_{\mathrm{f}}\tilde{\sigma}_{\mathrm{f},i}) \tag{11}$$

where $\tilde{\sigma}_{\mathrm{f},i} = \sigma_{\mathrm{fd},i} - \sigma_{\mathrm{f},i}$ is the time-varying formation task error, and λ_{f} is a positive gain. $J_{\mathrm{f},i}^{\dagger} = J_{\mathrm{f},i}^{\mathrm{T}}(J_{\mathrm{f},i}J_{\mathrm{f},i}^{\mathrm{T}})^{-1}$ is the pseudo inverse of the behavior-based Jacobian matrix $J_{\mathrm{f},i} = \left[\frac{\partial p_i}{\partial p_{i,1}}, \frac{\partial p_i}{\partial p_{i,2}}, \frac{\partial p_i}{\partial p_{i,3}}\right]^{\mathrm{T}}$ with $p_i = [p_{i,1}, p_{i,2}, p_{i,3}]^{\mathrm{T}}$.

Remark 1: From (8)–(10), it can be seen that only the neighborhood agents' information is needed, and thus, the proposed method is fully distributed rather than centralized control. In addition, the existing NSB control methods in [16], [17], [18], and [19] only considered the time-invariant formation, and the coordination between followers was ignored. For example, the formation task function was designed as $\rho_{\varsigma} = [(x_1 - x_b)^{\mathrm{T}}, \ldots, (x_n - x_b)^{\mathrm{T}}]^{\mathrm{T}}$ without considering adjustable coordination performance in [19], and the global information was requisite due to the term $x_b = \frac{1}{n}\sum_{i=1}^{n} x_i$. As shown in (9), however, the numerator of $\sigma_{\mathrm{fd},i}$ is composed of two parts with different weight coefficients: one realizes the tracking performance, and the other achieves the coordination with neighborhood agents. Then, the desired time-varying formation coordinate of follower i is obtained by the weighted average operation of the two parts. Clearly, if $\varrho_1 = 1$ and $\varrho_2 = 0$, only the tracking performance is considered, and if $\varrho_1 = 0$ and $\varrho_2 = 1$, only the coordination performance can be guaranteed. As a result, the proposed time-varying formation task strategy is flexible, and the parameters ϱ_1 and ϱ_2 can be chosen according to the needs of designers.

Define the CA task function as follows:

$$\sigma_{\mathrm{ca},i} = R - R\sin\left(\frac{\|p_i - p_i^{\mathrm{ca}}\|_2 + R - 4r}{2(R-2r)}\pi\right) \tag{12}$$

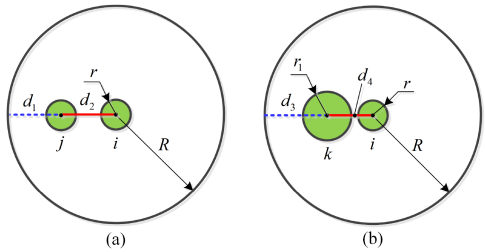

Fig. 2. Schematic diagram of CA.

where r is the radius of all ball-like agents, R is the radius of the collision warning area satisfying $R > 2r$, and p_i^{ca} is the coordinate of the center of the agent closest to agent i. The desired velocity for CA is

$$v_{\text{ca},i} = J_{\text{ca},i}^{\dagger} \lambda_{\text{ca}} \tilde{\sigma}_{\text{ca},i} \tag{13}$$

where $\tilde{\sigma}_{\text{ca},i} = \sigma_{\text{ca},i}^{*} - \sigma_{\text{ca},i}$ is the CA task error, and $\sigma_{\text{ca},i}^{*} = R$ is the fictitious sphere, λ_{ca} is a positive gain, which is large enough in terms of actuator constraint, and $J_{\text{ca},i}^{\dagger} = J_{\text{ca},i}^{\text{T}}(J_{\text{ca},i}J_{\text{ca},i}^{\text{T}})^{-1}$ with

$$J_{\text{ca},i} = \frac{-R\pi(p_i - p_i^{\text{ca}})^{\text{T}}}{2(R-2r)\|p_i - p_i^{\text{ca}}\|_2} \cos\left(\frac{\|p_i - p_i^{\text{ca}}\|_2 + R - 4r}{2(R-2r)}\pi\right). \tag{14}$$

Remark 2: In [16], [17], [18], [19], and [20], the desired velocity for CA task was only related to the distance d_1 or $d_1 - r$, as shown in Fig. 2(a), but in fact, collision risk is determined by the distance $d_2 - 2r$. For further illustration, the CA case between agents i and k is considered in Fig. 2(b), as a comparison with that between agents i and j. It is clear that if $d_1 - r = d_3 - r_1$, the same desired velocity for the CA task is obtained according to the CA algorithms in [16], [17], [18], [19], and [20]. Thus, the collision risk between agents i and k is greater than that between agents i and j since $r_1 > r$, and a greater desired velocity should be obtained due to $d_2 - 2r > d_4 - r - r_1$. Therefore, it is necessary to design a CA task function such that the desired velocity is directly determined by the distance $d_2 - 2r$ in Fig. 2(a). Also, the radius of agents is introduced into (12) such that the proposed method is more suitable for agents with different sizes in practical applications. Furthermore, when the CA task function (12) is active, that is, $2r < \|p_i - p_i^{\text{ca}}\|_2 \leq R$, $v_{\text{ca},i}$ approaches the maximum value as $\|p_i - p_i^{\text{ca}}\|_2 \to 2r$, and thus, collision risk can be exactly characterized by $\|p_i - p_i^{\text{ca}}\|_2 - 2r$ in this article instead of $R - \|p_i - p_i^{\text{ca}}\|_2 - r$ in [16], [17], [18], [19], [20]. Thus, the CA task is effectively constructed.

Remark 3: In (12), p_i^{ca} is assumed to be a static ball-like obstacle to obtain the concise algorithms (13) and (14), which is common (see [16] and [17]) and reasonable in practical applications. When the coordinate of agent j is treated as p_i^{ca}, the desired velocity $v_{\text{ca},i}$ will be generated to make agent i away from agent j. Also, similar algorithms are performed in agent j, and thus, the CA between agents i and j is achieved. With the constant p_i^{ca}, the complicated calculation coming from (13) and (14) is avoided, which is helpful for agents with limited energy. If p_i^{ca} in (12) is time-varying, (13) and (14), as well as the subsequent theoretical analysis, need some minor improvements by combining the proposed task function and the results in [20]. As an extension, the obstacle avoidance task function for dot-like and/or linear obstacles can be designed as $\sigma_{\text{oa},i} = R - R\sin\left(\frac{\|p_i - p_i^{\text{oa}}\|_2 + R - 2r}{2(R-r)}\pi\right)$, where p_i^{oa} is the coordinate of the closest point of the obstacle to agent i. In practice, agents are generally equipped with proper detection devices (e.g., lidars or cameras) to obtain the positions of obstacles.

With the null space projection between the time-varying formation and CA tasks [17], [18], [19], the desired velocity trajectory is obtained by using (11) and (13) as follows:

$$v_{\text{d},i} = v_{\text{ca},i} + (I_3 - J_{\text{ca},i}^{\dagger} J_{\text{ca},i}) v_{\text{f},i}. \tag{15}$$

Then, the desired position trajectory $p_{\text{d},i}$ can be obtained by taking the time integration of $v_{\text{d},i}$.

For the desired velocity trajectory design, the following result is derived.

Theorem 1: Considering the MAS (2) with the task design algorithm (8)–(15), the desired velocity trajectory generation maintains stable. Furthermore, the task errors $\tilde{\sigma}_{\text{f},i}$ and $\tilde{\sigma}_{\text{ca},i}$ satisfy that $\sum_{i=1}^{N} \|\tilde{\sigma}_{\text{f},i}\|_2^2$ and $\sum_{i=1}^{N} \|\tilde{\sigma}_{\text{ca},i}\|_2^2$ are bounded.

Proof: Define the following Lyapunov function candidate:

$$V_\sigma = \frac{1}{2}\sum_{i=1}^{N} (\gamma_{\text{ca}} \tilde{\sigma}_{\text{ca},i}^2 + \gamma_{\text{f}} \tilde{\sigma}_{\text{f},i}^{\text{T}} \tilde{\sigma}_{\text{f},i}) \tag{16}$$

where $\gamma_{\text{ca}} > 0$ and $\gamma_{\text{f}} > 0$.

When the distances between agents are all greater than R, the CA task is not activated, and we have $J_{\text{f},i} J_{\text{ca},i}^{\dagger} = 0$. Then, the derivative of V_σ is

$$\begin{aligned}
\dot{V}_\sigma &= \sum_{i=1}^{N} (\gamma_{\text{ca}} \tilde{\sigma}_{\text{ca},i} \dot{\tilde{\sigma}}_{\text{ca},i} + \gamma_{\text{f}} \tilde{\sigma}_{\text{f},i}^{\text{T}} \dot{\tilde{\sigma}}_{\text{f},i}) \\
&= \sum_{i=1}^{N} \left(\gamma_{\text{ca}} \tilde{\sigma}_{\text{ca},i} (\dot{\sigma}_{\text{ca},i}^{*} - \dot{\sigma}_{\text{ca},i}) + \gamma_{\text{f}} \tilde{\sigma}_{\text{f},i}^{\text{T}} (\dot{\sigma}_{\text{fd},i} - \dot{\sigma}_{\text{f},i})\right) \\
&= -\sum_{i=1}^{N} (\gamma_{\text{ca}} \tilde{\sigma}_{\text{ca},i} J_{\text{ca},i} v_{\text{d},i} + \gamma_{\text{f}} \tilde{\sigma}_{\text{f},i}^{\text{T}} J_{\text{f},i} v_{\text{d},i}) + \sum_{i=1}^{N} \gamma_{\text{f}} \tilde{\sigma}_{\text{f},i}^{\text{T}} \dot{\sigma}_{\text{fd},i} \\
&= -\sum_{i=1}^{N} \Big(\gamma_{\text{ca}} \tilde{\sigma}_{\text{ca},i} J_{\text{ca},i} \Big((I_3 - J_{\text{ca},i}^{\dagger} J_{\text{ca},i}) J_{\text{f},i}^{\dagger} \lambda_{\text{f}} \tilde{\sigma}_{\text{f},i} \\
&\quad + J_{\text{ca},i}^{\dagger} \lambda_{\text{ca}} \tilde{\sigma}_{\text{ca},i}\Big) + \gamma_{\text{f}} \tilde{\sigma}_{\text{f},i}^{\text{T}} J_{\text{f},i} \Big(J_{\text{ca},i}^{\dagger} \lambda_{\text{ca}} \tilde{\sigma}_{\text{ca},i} \\
&\quad + (I_3 - J_{\text{ca},i}^{\dagger} J_{\text{ca},i}) J_{\text{f},i}^{\dagger} \lambda_{\text{f}} \tilde{\sigma}_{\text{f},i}\Big)\Big) + \sum_{i=1}^{N} \gamma_{\text{f}} \tilde{\sigma}_{\text{f},i}^{\text{T}} \dot{\sigma}_{\text{fd},i} \\
&= -\sum_{i=1}^{N} (\lambda_{\text{ca}} \gamma_{\text{ca}} \tilde{\sigma}_{\text{ca},i}^2 + \lambda_{\text{f}} \gamma_{\text{f}} \tilde{\sigma}_{\text{f},i}^{\text{T}} \tilde{\sigma}_{\text{f},i}) + \sum_{i=1}^{N} \gamma_{\text{f}} \tilde{\sigma}_{\text{f},i}^{\text{T}} \dot{\sigma}_{\text{fd},i} \\
&\leq -2\min\{\lambda_{\text{ca}}, \lambda_{\text{f}}\} V_\sigma + M
\end{aligned} \tag{17}$$

where $\dot{p}_i = v_{\text{d},i}$ is used and its interpretation refers to [13]. M is an existing constant such that the inequality $M \geq \sum_{i=1}^{N} \gamma_{\text{f}} \tilde{\sigma}_{\text{f},i}^{\text{T}} \dot{\sigma}_{\text{fd},i}$ holds because of the bounded $\dot{\delta}_{\text{p}i}$ and $\dot{v}_{0,i}$.

Integrating the both sides of (17) yields

$$V_\sigma(t) \le \left(V_\sigma(0) - \frac{M}{2\min\{\lambda_{\rm ca},\lambda_{\rm f}\}}\right) e^{-2\min\{\lambda_{\rm ca},\lambda_{\rm f}\}t} + \frac{M}{2\min\{\lambda_{\rm ca},\lambda_{\rm f}\}} \le V_\sigma(0) \tag{18}$$

where $V_\sigma(0)$ is the initial value of V_σ. Then, we have $\sum_{i=1}^N \|\tilde\sigma_{{\rm f},i}\|_2^2 \le 2V_\sigma(0)/\gamma_{\rm f}$ and $\sum_{i=1}^N \|\tilde\sigma_{{\rm ca},i}\|_2^2 \le 2V_\sigma(0)/\gamma_{\rm ca}$.

When there is a conflict between the time-varying formation task and the CA task, the derivative of V_σ is

$$\begin{aligned}\dot V_\sigma \le & \sum_{i=1}^N \Big(-\gamma_{\rm f}\tilde\sigma_{{\rm f},i}^{\rm T}(J_{{\rm f},i}J_{{\rm f},i}^\dagger\lambda_{\rm f} - J_{{\rm f},i}J_{{\rm ca},i}^\dagger J_{{\rm ca},i}J_{{\rm f},i}^\dagger\lambda_{\rm f})\tilde\sigma_{{\rm f},i} \\ & - \gamma_{\rm ca}\lambda_{\rm ca}\tilde\sigma_{{\rm ca},i}^2 + \frac{1}{2}\gamma_{\rm f}\lambda_{\rm ca}\|J_{{\rm f},i}\|_2\|J_{{\rm ca},i}^\dagger\|_2(\tilde\sigma_{{\rm ca},i}^2 + \|\tilde\sigma_{{\rm f},i}\|_2^2)\Big) \\ & + \sum_{i=1}^N \gamma_{\rm f}\tilde\sigma_{{\rm f},i}^{\rm T}\dot\sigma_{{\rm fd},i} \\ \le & \sum_{i=1}^N \left(-\left(\gamma_{\rm ca} - \frac{1}{2}\gamma_{\rm f}\|J_{{\rm ca},i}^\dagger\|_2\right)\lambda_{\rm ca}\tilde\sigma_{{\rm ca},i}^2 \right. \\ & \left. + \frac{1}{2}\gamma_{\rm f}\lambda_{\rm ca}\|J_{{\rm ca},i}^\dagger\|_2\|\tilde\sigma_{{\rm f},i}\|_2^2\right) + \sum_{i=1}^N \gamma_{\rm f}\tilde\sigma_{{\rm f},i}^{\rm T}\dot\sigma_{{\rm fd},i}\end{aligned} \tag{19}$$

where $\|J_{{\rm f},i}\|_2 = 1$ is used, and $\gamma_{\rm ca} \ge \frac{1}{2}\gamma_{\rm f}\|J_{{\rm ca},i}^\dagger\|_2$ is prerequisite.

Similar to [16], [17], and [18], since the CA task, rather than the time-varying formation task, must be first guaranteed in the presence of collision risk, V_σ is redefined as $V_\sigma = \frac{1}{2}\sum_{i=1}^N \gamma_{\rm ca}\tilde\sigma_{{\rm ca},i}^2$, and its derivative satisfies $\dot V_\sigma = -\sum_{i=1}^N \gamma_{\rm ca}\lambda_{\rm ca}\|\tilde\sigma_{{\rm ca},i}\|_2^2 \le 0$, and then, the similar convergence properties and stability can be obtained as the aforementioned collision-free case, which completes the proof.

B. Controller Design for Fixed-Time Trajectory Tracking

With the desired position trajectory obtained abovementioned, the tracking error for follower i is defined as follows:

$$\begin{cases} e_{i,1} = p_i - p_{{\rm d},i} \\ e_{i,2} = v_i - v_{{\rm d},i} \end{cases} \tag{20}$$

where $e_{i,1}$ and $e_{i,2}$ are the position and velocity tracking errors, respectively. From (2) and (20), we have

$$\begin{cases} \dot e_{i,1} = e_{i,2} \\ \dot e_{i,2} = f(x_i) + g(x_i)u_i + d_i - \dot v_{{\rm d},i} \end{cases} \tag{21}$$

where $\|\dot v_{{\rm d},i}\|_1$ is assumed to be bounded satisfying $\|\dot v_{{\rm d},i}\|_1 \le \delta_2$, and δ_2 is a positive constant.

Remark 4: Based on (11), (13), and (15), with the properties of the norm, it can be ensured that $\|\dot v_{{\rm d},i}\|_1$ is bounded with appropriate u_0 and $\delta_{\rm p}$.

Inspired by Moulay et al. [24], two robust fixed-time sliding mode controllers are designed by using constant and variable exponent coefficients.

First, the constant exponent coefficient case is considered, and a sliding surface is constructed as follows:

$$s_i = e_{i,2} + \beta e_{i,1} \tag{22}$$

where $\beta > 0$. Then, the sliding mode tracking controller is

$$\begin{aligned}u_i = & -g^{-1}(x_i)\left(f(x_i) + \beta e_{i,2} + k_1{\rm sign}(s_i)\right. \\ & \left. + k_2\|s_i\|_2^\alpha{\rm sign}(s_i) + k_3\|s_i\|_2^\gamma{\rm sign}(s_i) + k_4 s_i\right)\end{aligned} \tag{23}$$

where $k_1 > \delta_1 + \delta_2$, $k_2 > 0$, $k_3 \ge 0$, $k_4 \ge 0$, $\alpha > 1$, and $0 < \gamma < 1$. Then, the trajectory tracking control problem is solved in the following theorem.

Theorem 2: Using the proposed control law (23) with (22), the global robust asymptotic stabilization is achieved for system (21) with the desired trajectory $p_{{\rm d},i}$ and $v_{{\rm d},i}$. In particular, the sliding manifold $s_i = 0$ is reached in a fixed time, and the settling time satisfies

$$T_1 \le \frac{1}{k_1 - \delta_1 - \delta_2} + \frac{1}{k_2 N^{1-\frac{\alpha+1}{2}}(\alpha - 1)}. \tag{24}$$

Proof: Consider the Lyapunov function candidate

$$V_{\rm s} = \sum_{i=1}^N s_i^{\rm T} s_i \tag{25}$$

and the derivative of $V_{\rm s}$ is

$$\begin{aligned}\dot V_{\rm s} = & 2\sum_{i=1}^N s_i^{\rm T}\left(-k_1{\rm sign}(s_i) - k_2\|s_i\|_2^\alpha{\rm sign}(s_i)\right. \\ & \left. - k_3\|s_i\|_2^\gamma{\rm sign}(s_i) - k_4 s_i + d_i - \dot v_{{\rm d},i}\right) \\ = & 2\sum_{i=1}^N\left(-k_1\|s_i\|_1 - k_2\|s_i\|_2^\alpha\|s_i\|_1 - k_3\|s_i\|_2^\gamma\|s_i\|_1\right. \\ & \left. - k_4\|s_i\|_2^2 + s_i^{\rm T}d_i - s_i^{\rm T}\dot v_{{\rm d},i}\right) \\ \le & 2\sum_{i=1}^N\left(-(k_1 - \delta_1 - \delta_2)\|s_i\|_1 - k_2\|s_i\|_2^\alpha\|s_i\|_1\right) \\ \le & 2\sum_{i=1}^N\left(-(k_1 - \delta_1 - \delta_2)\|s_i\|_2 - k_2\|s_i\|_2^{\alpha+1}\right) \\ \le & -2(k_1 - \delta_1 - \delta_2)V_{\rm s}^{\frac{1}{2}} - 2k_2 N^{1-\frac{\alpha+1}{2}}V_{\rm s}^{\frac{\alpha+1}{2}}\end{aligned} \tag{26}$$

where $\|s_i\|_1 \ge \|s_i\|_2$ and Lemma 2 are used. Then, according to Lemma 1, it is deduced that system (2) with (22) and (23) reaches the sliding surface $s_i = 0$ in a fixed time T_1 satisfying (24). When the sliding surface is reached, we get

$$\dot e_{i,1} = -\beta e_{i,1} \tag{27}$$

which guarantees the asymptotic stability of system (21). The proof is finished.

Remark 5: With (21) and (23), the derivative of (22) is

$$\begin{aligned}\dot s_i = & -k_1{\rm sign}(s_i) - k_2\|s_i\|_2^\alpha{\rm sign}(s_i) - k_3\|s_i\|_2^\gamma{\rm sign}(s_i) \\ & - k_4 s_i + d_i - \dot v_{{\rm d},i}.\end{aligned} \tag{28}$$

In (23), the term $k_1{\rm sign}(s_i)$ is used to deal with unknown d_i and $\dot v_{{\rm d},i}$, and combining with it, the term $k_2\|s_i\|_2^\alpha{\rm sign}(s_i)$ can drive

(28) to achieve fixed-time stability. It is easy to observe from (24) that, although the parameters k_3 and k_4 have no effect on the stability of (28), they can make controller (23) more flexible.

Second, to achieve both reaching phase and sliding motion in fixed time, the sliding surface with a state-dependent time-varying exponent coefficient is introduced as follows:

$$\tilde{s}_i = e_{i,2} + \beta^* \|e_{i,1}\|_2^{\frac{\lambda^*\|e_{i,1}\|_2^2}{1+\mu^*\|e_{i,1}\|_2^2}} \operatorname{sign}(e_{i,1}) \tag{29}$$

where $\beta^* > 0$, $\lambda^* > 0$, and $\mu^* > 0$ satisfying $\theta^* = \dfrac{\lambda^*}{1+\mu^*} > 1$. The corresponding controller is designed as follows:

$$\begin{aligned}\tilde{u}_i = & -g^{-1}(x_i)\Bigg(f(x_i) + k_1^*\operatorname{sign}(\tilde{s}_i) + k_2^*\|\tilde{s}_i\|_2^{\alpha^*}\operatorname{sign}(\tilde{s}_i) \\ & + \frac{\beta^*\lambda^* e_{i,1}^{\mathrm{T}} e_{i,2}}{1+\mu^*\|e_{i,1}\|_2^2}\left(\frac{2\ln(\|e_{i,1}\|_2)}{1+\mu^*\|e_{i,1}\|_2^2}+1\right) \\ & \times \|e_{i,1}\|_2^{\frac{\lambda^*\|e_{i,1}\|_2^2}{1+\mu^*\|e_{i,1}\|_2^2}}\operatorname{sign}(e_{i,1})\Bigg)\end{aligned} \tag{30}$$

where $k_1^* > \delta_1 + \delta_2$, $k_2^* > 0$, and $\alpha^* > 1$. With the fact that $\lim_{\|e_{i,1}\|_2\to 0} e_{i,1}^{\mathrm{T}} e_{i,2}\ln(\|e_{i,1}\|_2) = 0$, the singularity of (30) is, thus, eliminated. Similar to Theorem 2, the following theorem is obtained for the variable exponent coefficient case.

Theorem 3: With the desired trajectory $p_{\mathrm{d},i}$ and $v_{\mathrm{d},i}$, system (21) achieves global robust fixed-time stabilization by control law (30) with (29), and the settling time T_2 satisfies

$$\begin{aligned}T_2 \le & \frac{1}{k_1^*-\delta_1-\delta_2} + \frac{1}{k_2^* N^{1-\frac{\alpha^*+1}{2}}(\alpha^*-1)} \\ & + \frac{1}{\beta^* N^{1-\frac{\theta^*+1}{2}}(\theta^*-1)} + \frac{1}{\beta^* e^{\frac{-\lambda^*}{2e}}}.\end{aligned} \tag{31}$$

Proof: Consider the following Lyapunov function:

$$V_{\tilde{\mathrm{s}}} = \sum_{i=1}^{N} \tilde{s}_i^{\mathrm{T}}\tilde{s}_i.$$

Taking the derivative of $V_{\tilde{\mathrm{s}}}$ yields

$$\begin{aligned}\dot{V}_{\tilde{\mathrm{s}}} & \le 2\sum_{i=1}^{N}(-k_1^*\|\tilde{s}_i\|_1 - k_2^*\|\tilde{s}_i\|_2^{\alpha^*}\|\tilde{s}_i\|_1 + \delta_1\|\tilde{s}_i\|_1 + \delta_2\|\tilde{s}_i\|_1) \\ & \le 2\sum_{i=1}^{N}\left(-(k_1^*-\delta_1-\delta_2)\|\tilde{s}_i\|_2 - k_2^*\|\tilde{s}_i\|_2^{\alpha^*+1}\right) \\ & \le -2(k_1^*-\delta_1-\delta_2)V_{\tilde{\mathrm{s}}}^{\frac{1}{2}} - 2k_2^* N^{1-\frac{\alpha^*+1}{2}} V_{\tilde{\mathrm{s}}}^{\frac{\alpha^*+1}{2}}.\end{aligned}$$

Similar to the aforementioned constant exponent coefficient case, the sliding surface $\tilde{s}_i = 0$ is reached in the following fixed time:

$$T_{21} \le \frac{1}{k_1^*-\delta_1-\delta_2} + \frac{1}{k_2^* N^{1-\frac{\alpha^*+1}{2}}(\alpha^*-1)}.$$

When the sliding surface is reached, we have

$$\dot{e}_{i,1} = -\beta^*\|e_{i,1}\|_2^{\frac{\lambda^*\|e_{i,1}\|_2^2}{1+\mu^*\|e_{i,1}\|_2^2}}\operatorname{sign}(e_{i,1}). \tag{32}$$

For the system (32), consider the following Lyapunov function:

$$V_{\tilde{\mathrm{e}}} = \sum_{i=1}^{N} e_{i,1}^{\mathrm{T}} e_{i,1}.$$

Taking the time derivative of $V_{\tilde{\mathrm{e}}}$, one obtains

$$\begin{aligned}\dot{V}_{\tilde{\mathrm{e}}} & = -2\beta^*\sum_{i=1}^{N} e_{i,1}^{\mathrm{T}}\|e_{i,1}\|_2^{\frac{\lambda^*\|e_{i,1}\|_2^2}{1+\mu^*\|e_{i,1}\|_2^2}}\operatorname{sign}(e_{i,1}) \\ & = -2\beta^*\sum_{i=1}^{N}\|e_{i,1}\|_1\|e_{i,1}\|_2^{\frac{\lambda^*\|e_{i,1}\|_2^2}{1+\mu^*\|e_{i,1}\|_2^2}}.\end{aligned}$$

Next, two situations are discussed. When $\|e_{i,1}\|_2 \ge 1$, we have $\dfrac{\lambda^*\|e_{i,1}\|_2^2}{1+\mu^*\|e_{i,1}\|_2^2} + 1 \ge \dfrac{\lambda^*}{1+\mu^*} + 1 > 2$. Then,

$$\begin{aligned}\dot{V}_{\tilde{\mathrm{e}}} & \le -2\beta^*\sum_{i=1}^{N}\|e_{i,1}\|_2^{\frac{\lambda^*\|e_{i,1}\|_2^2}{1+\mu^*\|e_{i,1}\|_2^2}+1} \\ & \le -2\beta^*\sum_{i=1}^{N}\|e_{i,1}\|_2^{\theta^*+1} \\ & \le -2\beta^* N^{1-\frac{\theta^*+1}{2}} V_{\tilde{\mathrm{e}}}^{\frac{\theta^*+1}{2}}.\end{aligned}$$

According to ([24], Th. 2), all the solutions starting from $\{\|e_{i,1}\|_2 > 1\}$ reach the set $\{\|e_{i,1}\|_2 \le 1\}$ in a fixed time $T_{22} \le \dfrac{1}{\beta^* N^{1-\frac{\theta^*+1}{2}}(\theta^*-1)}$.

When $\|e_{i,1}\|_2 \le 1$, with $1+\mu^*\|e_{i,1}\|_2^2 \ge 1$, we obtain that $\min\left(\|e_{i,1}\|_2^{\frac{\lambda^*\|e_{i,1}\|_2^2}{1+\mu^*\|e_{i,1}\|_2^2}}\right) \ge \min\left(\|e_{i,1}\|_2^{\lambda^*\|e_{i,1}\|_2^2}\right) = e^{-\frac{\lambda^*}{2e}}$. Hence,

$$\begin{aligned}\dot{V}_{\tilde{\mathrm{e}}} & \le -2\beta^*\sum_{i=1}^{N}\|e_{i,1}\|_2\|e_{i,1}\|_2^{\frac{\lambda^*\|e_{i,1}\|_2^2}{1+\mu^*\|e_{i,1}\|_2^2}} \\ & \le -2\beta^* e^{-\frac{\lambda^*}{2e}} V_{\tilde{\mathrm{e}}}^{\frac{1}{2}}.\end{aligned}$$

Clearly, all the solutions starting from $\{\|e_{i,1}\|_2 \le 1\}$ reach the origin in a uniform time $T_{23} \le \dfrac{1}{\beta^* e^{\frac{-\lambda^*}{2e}}}$. Therefore, the global robust stabilization problem is solved in a fixed time $T_2 = T_{21} + T_{22} + T_{23}$. The proof is completed.

Remark 6: It is noted that only the robust fixed-time stability problem was addressed in [24] for scalar systems, and the results cannot be directly applied to multidimensional space. In this article, by utilizing the behavior control approach and the properties of norm inequalities, the results in [24] are extended to the time-varying formation tracking control scenario in multidimensional MASs. Furthermore, the results of the settling

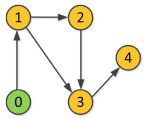

Fig. 3. Communication topology of an MAS.

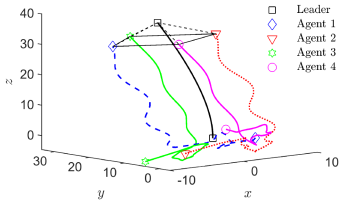

Fig. 4. Formation trajectories with CA.

time are derived, which are related to the number of agents, just as shown in (24) and (31). In addition, different from [19], two fixed-time control strategies are proposed with constant and variable exponent coefficients in multidimensional space, respectively.

IV. Simulation and Experimental Results

In this section, numerical simulation and practical experiments are conducted to verify the effectiveness and superiority of the proposed method. Due to the limited space, only the variable exponent coefficient case of the tracking controller is tested in the following simulation and experiment.

A. Simulation Results

An MAS with the communication topology in Fig. 3 is considered, and the simulation conditions are the same as those in [28], i.e., $u_0 = [0, \sin(0.1t), 0.5]^{\mathrm{T}}$, $f(x_i) = -0.1\sin(p_i) - 0.2v_i$, $g(x_i) = 1$, $d_i = [\sin(10t), \sin(10t), \sin(10t)]^{\mathrm{T}}$, $i = 1, 2, 3, 4$. The initial positions and velocities of agents are

$$\begin{cases} p_0(0) = [2, 10, 0]^{\mathrm{T}} \\ p_1(0) = [4, 2, 1]^{\mathrm{T}} \\ p_2(0) = [-6, 1, -1]^{\mathrm{T}} \\ p_3(0) = [-10, 4, -3]^{\mathrm{T}} \\ p_4(0) = [0, 2, 5]^{\mathrm{T}}, \end{cases} \quad \begin{cases} v_0(0) = [0, 0, 1]^{\mathrm{T}} \\ v_1(0) = [0.2, 1, 0]^{\mathrm{T}} \\ v_2(0) = [0, 0.4, 0]^{\mathrm{T}} \\ v_3(0) = [0.6, 2, -3]^{\mathrm{T}} \\ v_4(0) = [0.2, 1, 0]^{\mathrm{T}}. \end{cases}$$

The desired relative position are set as follows:

$$\begin{cases} \delta_{\mathrm{p1}} = [-7 + \sin(2t), 0, -6]^{\mathrm{T}} \\ \delta_{\mathrm{p2}} = [7 + \sin(2t), 0, -6]^{\mathrm{T}} \\ \delta_{\mathrm{p3}} = [0, 7 + \sin(2t), -6]^{\mathrm{T}} \\ \delta_{\mathrm{p4}} = [0, -7 + \sin(2t), -6]^{\mathrm{T}}. \end{cases}$$

The parameters of the proposed method in (8)–(13), (29), and (30) are chosen as $\lambda_{\mathrm{ca}} = 26$, $\lambda_{\mathrm{f}} = 0.8$, $c_1 = c_2 = 2$, $\beta^* = 1$, $\delta_2 = 10$, $\lambda^* = 1.6$, $\mu^* = 0.4$, $k_1^* = 15$, $k_2^* = 20$, $\alpha^* = 1.5$, $R = 5$, $\varrho_1 = 0.5$, $\varrho_2 = 0.5$, and $r = 1$.

The simulation results are shown in Figs. 4–6. It can be seen from Fig. 4 that the followers form a square formation to track the virtual leader, and the side length of the square is time-varying.

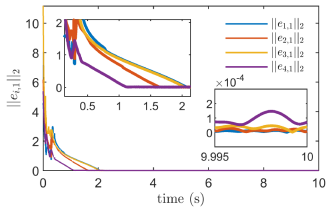

Fig. 5. Tracking errors with CA.

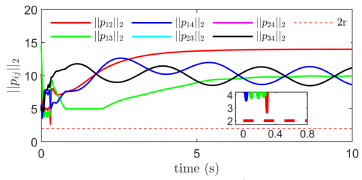

(a)

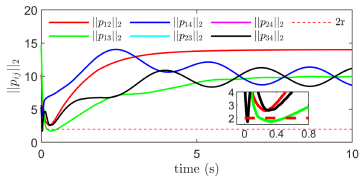

(b)

Fig. 6. Distances between agents with/without CA. (a) $\|p_{ij}\|2$ with CA. (b) $\|p_{ij}\|2$ without CA.

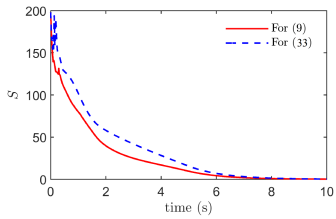

Fig. 7. Comparison of two time-varying formation task design methods.

Fig. 5 shows that the 2-norms of tracking errors converge rapidly to a specified domain in fixed time T_2. Fig. 6 gives the distances between followers with and without CA, which indicate that a collision-free formation is achieved in the presence of task conflict.

For comparison, the simulation is carried out for the formation method in [16] with the following desired coordinate of follower i:

$$\sigma_{\mathrm{fd},i}^* = \hat{p}_{0,i} + \delta_{\mathrm{p}i},\ i = 1, 2, 3, 4. \tag{33}$$

With $\bar{e}_i = \sum_{j=1, j\neq i}^{4} \|p_i - \delta_{\mathrm{p}i} - (p_j - \delta_{\mathrm{p}j})\|_2$, the variable $S = \sum_{i=1}^{4} \bar{e}_i$ is served as a performance indicator, of which the simulation are drawn in Fig. 7 for the proposed method and the method in [16]. It is obtained that $\sum_{t=0}^{10} S$ is 2.4683×10^6 and 3.3603×10^6 for the two cases, respectively, which indicates that a better coordination performance is achieved by using the proposed method.

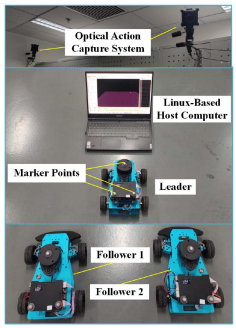

Fig. 8. Experimental platform.

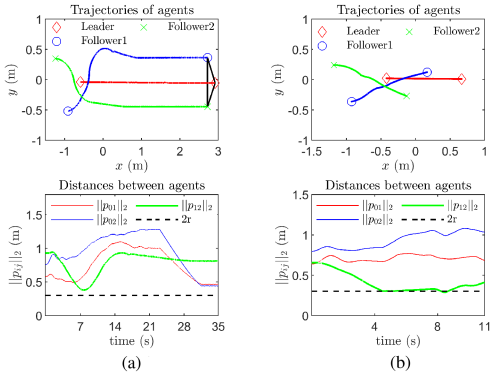

Fig. 9. Experimental results with/without CA. (a) With CA. (b) Without CA.

B. Experimental Results

An experimental platform is built to further demonstrate the effectiveness and feasibility of the proposed formation control scheme, as shown in Fig. 8, which mainly consists of an optical action capture system (i.e., a camera-based positioning system), a Linux-based host computer, and three small vehicles equipped with a robot operating system (ROS). The software named Seeker and four cameras with resolution of 12 MP and frequency of 300 Hz are the main components of the positioning system. When the vehicles with marker points are located in the workspace, they are captured by the cameras such that their absolute positions and velocities with respect to the global coordinate system, as well as other relative kinematic data, are obtained after calculation and analysis. The Linux-based host computer receives position and velocity information from cameras, and then transmits data to vehicles. Based on the obtained data and the proposed method, the control inputs produced in ROS are applied to vehicles.

The vehicles are considered as the ball-like agents with $r = 0.15$and $R = 0.35$ m, and two experiments are performed. One is the fixed formation with CA, and the other is the time-varying formation with obstacle avoidance. In the two experiments, one of the three vehicles acts as the leader, and the other two vehicles are the followers. Furthermore, the communication topology is directed, where only follower 1 can receive information from the leader, and follower 2 can obtain information from follower 1. The leader is autonomous and moves along a straight line with a constant speed $v_0 = 0.1$m/s. The control target is that the followers track the leader, while maintaining a prescribed formation. Since the dynamic of each vehicle can be approximated as a double integral system, the controller parameters in the simulation part are used for the practical experiments.

The desired formation shapes for the formation experiments are described as follows:

$$\begin{cases} \delta_{\mathrm{p}1}^{\mathrm{f}} = [-0.2, 0.4]^{\mathrm{T}} \\ \delta_{\mathrm{p}2}^{\mathrm{f}} = [-0.2, -0.4]^{\mathrm{T}} \end{cases}$$

$$\begin{cases} \delta_{\mathrm{p}1}^{\mathrm{t}} = [-0.2, 0.25 + 0.15\sin(0.5t + 1.5)]^{\mathrm{T}},\ 0 < t < 14 \\ \delta_{\mathrm{p}1}^{\mathrm{t}} = [-0.2, 0.5]^{\mathrm{T}},\ t \geq 14 \\ \delta_{\mathrm{p}2}^{\mathrm{t}} = [-0.2, -0.8 - 0.15\sin(0.5t + 1.5)]^{\mathrm{T}},\ 0 < t < 14 \\ \delta_{\mathrm{p}2}^{\mathrm{t}} = [-0.2, -0.5]^{\mathrm{T}},\ t \geq 14 \end{cases}$$

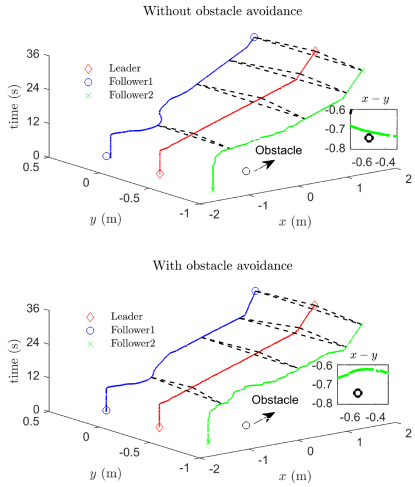

Fig. 10. Formation trajectories with/without obstacle avoidance.

where $\delta_{\mathrm{p}i}^{\mathrm{f}}$ and $\delta_{\mathrm{p}i}^{\mathrm{t}}$ denote the desired position offsets for the fixed and time-varying formation, respectively, $i = 1, 2$. The corresponding experimental results are shown in Figs. 9 and 10, respectively. As illustrated in Fig. 9(a), three vehicles start from their respective initial positions, and eventually form a triangular formation. The evolution of the distances between vehicles indicates that collision does not occur because of $\|p_{ij}\|_2 > 2r$. On the contrary, without CA, follower 1 collides with follower 2 at time $t = 4.47$ s, and then the trajectories of three vehicles become chaotic [see Fig. 9(b)]. It is worth pointing out that in Fig. 9, only the experimental result of 11 s [less than 35 s in Fig. 9(b)] is presented because followers 1 and 2 are hard to separate after the collision. In addition, the distance between followers 1 and 2 cannot be less than $2r$ after the collision in the experiment, unless they are deformed. Fig. 10 shows that the formation shape is time-varying. Furthermore, from the comparison of the upper and lower figures of Fig. 10, it is easy to see that follower 2 has notable actions to avoid an obstacle.

V. Conclusion

In this article, the problem of time-varying formation control was studied for uncertain nonlinear second-order MASs in an NSB architecture. Novel time-varying formation task and collision avoidance task strategies were designed to generate the desired motion trajectory. Subsequently, sliding-mode tracking controllers were designed for constant and state-dependent variable exponent coefficient cases, respectively. Then, the theoretical analysis was made for the desired trajectory generation and the fixed-time trajectory tracking. Finally, both the simulation and experimental results were presented to illustrate the validity and applicability of the proposed method. It is noted that mismatched disturbance was not considered in this article [29]. In addition, the cooperation between agents was generally achieved via networks, and thus, some communication constraints, such as network delays, packet dropouts, and even cyber-attacks, were inevitable in practical applications [30], [31], [32]. These issues will be addressed in our future work to further extend the proposed method.

References

[1] X. Dong and G. Hu, "Time-varying formation tracking for linear multiagent systems with multiple leaders," *IEEE Trans. Autom. Control*, vol. 62, no. 7, pp. 3658–3664, Jul. 2017.

[2] S. Zuo, Y. Song, F. L. Lewis, and A. Davoudi, "Time-varying output formation containment of general linear homogeneous and heterogeneous multiagent systems," *IEEE Trans. Control Netw. Syst.*, vol. 6, no. 2, pp. 537–548, Jun. 2019.

[3] Z.-H. Pang, C.-B. Zheng, C. Li, G.-P. Liu, and Q.-L. Han, "Cloud-based time-varying formation predictive control of multi-agent systems with random communication constraints and quantized signals," *IEEE Trans. Circuits Syst. II Exp. Briefs*, vol. 69, no. 3, pp. 1282–1286, Mar. 2022.

[4] C. Yan, W. Zhang, H. Su, and X. Li, "Adaptive bipartite time-varying output formation control for multiagent systems on signed directed graphs," *IEEE Trans. Cybern.*, vol. 52, no. 9, pp. 8987–9000, Sep. 2022.

[5] L. Dai, Q. Cao, Y. Xia, and Y. Gao, "Distributed MPC for formation of multiagent systems with collision avoidance and obstacle avoidance," *J. Franklin Inst.*, vol. 354, no. 4, pp. 2068–2085, Mar. 2017.

[6] H. Yang, Q. Li, Z. Zuo, and H. Zhao, "Event-triggered model predictive control for multi-vehicle systems with collision avoidance and obstacle avoidance," *Int. J. Robust Nonlinear Control*, vol. 31, no. 11, pp. 5476–5494, Jul. 2021.

[7] G. Yu, P. K. Wong, J. Zhao, X. Mei, C. Lin, and Z. Xie, "Design of an acceleration redistribution cooperative strategy for collision avoidance system based on dynamic weighted multiobjective model predictive controller," *IEEE Trans. Intell. Transp. Syst.*, vol. 23, no. 6, pp. 5006–5018, Jun. 2022.

[8] Q. Li, J. Yuan, B. Zhang, and H. Wang, "Artificial potential field based robust adaptive control for spacecraft rendezvous and docking under motion constraint," *ISA Trans.*, vol. 95, pp. 173–184, Jan. 2019.

[9] Z.-H. Pang, C.-B. Zheng, J. Sun, Q.-L. Han, and G.-P. Liu, "Distance- and velocity-based collision avoidance for time-varying formation control of second-order multiagent systems," *IEEE Trans. Circuits Syst. II Exp. Briefs*, vol. 68, no. 4, pp. 1253–1257, Apr. 2021.

[10] Z. S. Lippay and J. B. Hoagg, "Formation control with time-varying formations, bounded controls, and local collision avoidance," *IEEE Trans. Control Syst. Technol.*, vol. 30, no. 1, pp. 261–276, Jan. 2022.

[11] G. Antonelli, F. Arrichiello, and S. Chiaverini, "Experiments of formation control with collisions avoidance using the null-space-based behavioral control," in *Proc. 14th Mediterr. Conf. Control Autom.*, 2006, Art. no. 1700798.

[12] F. Arrichiello, S. Chiaverini, and T. I. Fossen, "Formation control of underactuated surface vessels using the null-space-based behavioral control," in *Proc. IEEE Int. Conf. Intell. Robots Syst.*, 2006, pp. 5942–5947.

[13] G. Antonelli, "Stability analysis for prioritized closed-loop inverse kinematic algorithms for redundant robotic systems," *IEEE Trans. Robot.*, vol. 25, no. 5, pp. 985–994, Oct. 2009.

[14] M. C. P. Santos, C. D. Rosales, M. Sarcinelli-Filho, and R. Carelli, "A novel null-space-based UAV trajectory tracking controller with collision avoidance," *IEEE/ASME Trans. Mechatron.*, vol. 22, no. 6, pp. 2543–2553, Dec. 2017.

[15] R. Schlanbusch, R. Kristiansen, and P. J. Nicklasson, "Spacecraft formation reconfiguration with collision avoidance," *Automatica*, vol. 47, no. 7, pp. 1443–1449, Jul. 2011.

[16] W. Wang, C. Li, and Y. Guo, "Relative position coordinated control for spacecraft formation flying with obstacle/collision avoidance," *Nonlinear Dyn.*, vol. 104, pp. 1329–1342, Mar. 2021.

[17] N. Zhou and Y. Xia, "Coordination control design for formation reconfiguration of multiple spacecraft," *IET Control Theory Appl.*, vol. 9, no. 15, pp. 2222–2231, Oct. 2015.

[18] J. Chen, M. Gan, J. Huang, L. Dou, and H. Fang, "Formation control of multiple euler-lagrange systems via null-space-based behavioral control," *Sci. China Inf. Sci.*, vol. 59, no. 1, pp. 1–11, Jan. 2016.

[19] J. Huang, N. Zhou, and M. Cao, "Adaptive fuzzy behavioral control of second-order autonomous agents with prioritized missions: Theory and experiments," *IEEE Trans. Ind. Electron.*, vol. 66, no. 12, pp. 9612–9622, Dec. 2019.

[20] N. Zhou, X. Cheng, Z. Sun, and Y. Xia, "Fixed-time cooperative behavioral control for networked autonomous agents with second-order nonlinear dynamics," *IEEE Trans. Cybern.*, vol. 52, no. 9, pp. 9504–9518, Sep. 2022.

[21] Z. Zuo, Q.-L. Han, B. Ning, X. Ge, and X.-M. Zhang, "An overview of recent advances in fixed-time cooperative control of multiagent systems," *IEEE Trans. Ind. Informat.*, vol. 14, no. 6, pp. 2322–2334, Jun. 2018.

[22] M. L. Corradini and A. Cristofaro, "Nonsingular terminal sliding-mode control of nonlinear planar systems with global fixed-time stability guarantees," *Automatica*, vol. 95, pp. 561–565, Sep. 2018.

[23] S. Shi, J. Gu, S. Xu, and H. Min, "Variable-gain second-order sliding mode controller with globally fixed-time stability guarantees," *IEEE Trans. Circuits Syst. II Exp. Briefs*, vol. 67, no. 8, pp. 1414–1418, Aug. 2020.

[24] E. Moulay, V. Léchappé, E. Bernuau, and F. Plestan, "Robust fixed-time stability: Application to sliding mode control," *IEEE Trans. Autom. Control*, vol. 67, no. 2, pp. 1061–1066, Feb. 2022.

[25] Z. Zuo, Q.-L. Han, and B. Ning, *Fixed-Time Cooperative Control of Multi-Agent Systems*. Cham, Switzerland: Springer, 2019.

[26] Q. Li, J. Wei, Q. Gou, and Z. Niu, "Distributed adaptive fixed-time formation control for second-order multiagent systems with collision avoidance," *Inf. Sci.*, vol. 564, pp. 27–44, Jul. 2021.

[27] Y. Cao, W. Ren, and Z. Meng, "Decentralized finite-time sliding mode estimators and their applications in decentralized finite-time formation tracking," *Syst. Control Lett.*, vol. 59, no. 9, pp. 522–529, Sep. 2010.

[28] D. Yao, H. Li, R. Lu, and Y. Shi, "Distributed sliding-mode tracking control of second-order nonlinear multiagent systems: An event-triggered approach," *IEEE Trans. Cybern.*, vol. 50, no. 9, pp. 3892–3902, Sep. 2020.

[29] J. Ke, W. Huang, J. Wang, and J. Zeng, "Fixed-time consensus control for multiagent systems with prescribed performance under matched and mismatched disturbances," *ISA Trans.*, vol. 119, pp. 135–151, Jan. 2022.

[30] Z.-H. Pang, W.-C. Luo, G.-P. Liu, and Q.-L. Han, "Observer-based incremental predictive control of networked multiagent systems with random delays and packet dropouts," *IEEE Trans. Circuits Syst. II Exp. Briefs*, vol. 68, no. 1, pp. 426–430, Jan. 2021.

[31] Z.-H. Pang, X.-Y. Zhao, J. Sun, Y. Shi, and G.-P. Liu, "Comparison of three data-driven networked predictive control methods for a class of nonlinear systems," *IEEE/CAA J. Autom. Sin.*, vol. 9, no. 9, pp. 1714–1716, Sep. 2022.

[32] Z.-H. Pang, L.-Z. Fan, J. Sun, K. Liu, and G.-P. Liu, "Detection of stealthy false data injection attacks against networked control systems via active data modification," *Inf. Sci.*, vol. 546, pp. 192–205, Feb. 2021.

Chang-Bing Zheng received the B.Eng. degree in electrical engineering and automation from the Wanfang School of Science and Technology, Henan Polytechnic University, Jiaozuo, China, in 2012, and the M.Eng. degree in in control science and engineering from the School of Electrical and Control Engineering, North China University of Technology, Beijing, China, in 2015, where he is currently working toward the Ph.D. degree in control science and engineering.

His current research interests include multiagent systems and networked control systems.

Zhong-Hua Pang (Senior Member, IEEE) received the B.Eng. degree in automation and M.Eng. degree in control theory and control engineering from the Qingdao University of Science and Technology, Qingdao, China, in 2002 and 2005, respectively, and the Ph.D. degree in control theory and control engineering from the Institute of Automation, Chinese Academy of Sciences, Beijing, China, in 2011.

From September 2011 to February 2014, he was a Postdoctoral Research Fellow with Tsinghua University, Beijing, China, a Visiting Scholar with the University of South Wales, Caerleon, U.K., from November 2016 to October 2017 and with the Swinburne University of Technology, Hawthorn, VIC, Australia, from July 2019 to August 2019 and from January 2020 to March 2020. Since 2014, he has been with the North China University of Technology, Beijing, China, first as an Associate Professor and, since 2017, as a Professor. His research interests include networked control systems, multiagent systems, security of cyber-physical systems, and data-driven control systems.

Jing-Xu Wang received the B.Eng. degree in automation and M.Eng. degree in control science and engineering from the North China University of Technology, Beijing, China, in 2021, where he is currently working toward the Postgraduate degree in control science and engineering.

His current research interest is multiagent systems and networked control systems.

Jian Sun (Senior Member, IEEE) received the B.Eng. degree in electrical engineering from the Jilin Institute of Technology, Jilin, China, in 2001, the M.Eng. degree in electrical engineering from the Changchun Institute of Optics, Fine Mechanics and Physics, Chinese Academy of Sciences (CAS), Beijing, China, in 2004, and the Ph.D. degree in control theory and control engineering from the Institute of Automation, CAS, in 2007.

From 2008 to 2009, he was a Research Fellow with the University of Glamorgan, Pontypridd, U.K. From 2007 to 2010, he was a Postdoctoral Research Fellow with the Beijing Institute of Technology, Beijing, China. In 2010, he joined the School of Automation, Beijing Institute of Technology, where he has been a Professor since 2013. His current research interests include networked control systems, time-delay systems, and security of cyber-physical systems.

Dr. Sun is an Editorial Board Member of the IEEE TRANSACTIONS ON SYSTEMS, MAN AND CYBERNETICS: SYSTEMS and *Journal of Systems Science and Complexity*.

Guo-Ping Liu (Fellow, IEEE) received the B.Eng. degree in industrial automation and M.Eng. degree in control engineering from the Central South University of Technology, Changsha, China, in 1982 and 1985, respectively, and the Ph.D. degree in control systems from the University of Manchester, Manchester, U.K., in 1992.

He is currently a Professor with the Southern University of Science and Technology, Shenzhen, China. His research interests include networked multiagent control, nonlinear identification and intelligent control, multiobjective optimal control, and industrial advanced control applications.

Dr. Liu was the General Chair of the 2007 IEEE International Conference on Networking, Sensing and Control, 2011 International Conference on Intelligent Control and Information Processing, and 2012 UKACC International Conference on Control. He was an Editor-in-Chief of the *International Journal of Automation and Computing* in 2004–2021. He is a Member of the Academy of Europe, Fellow of IET and CAA.

Qing-Long Han (Fellow, IEEE) received the B.Sc. degree in mathematics from Shandong Normal University, Jinan, China, in 1983, and the M.Sc. and Ph.D. degrees in control engineering from the East China University of Science and Technology, Shanghai, China, in 1992 and 1997, respectively.

He is currently the Pro Vice-Chancellor (Research Quality) and a Distinguished Professor with the Swinburne University of Technology, Hawthorn, VIC, Australia. He held various academic and management positions with Griffith University and Central Queensland University, Rockhampton, QLD, Australia. His research interests include networked control systems, multiagent systems, time-delay systems, smart grids, unmanned surface vehicles, and neural networks.

Dr. Han is a Member of the Academy of Europe, and a Fellow of IFAC andIEAust. He is a Highly Cited Researcher in both engineering and computer science (Clarivate Analytics). He was an AdCom Member of IEEE IES, IEEE IES Fellows Committee, and the Chair of IEEE IES Technical Committee on Networked Control Systems. He is the Co-Editor-in-Chief of IEEE TRANSACTIONS ON INDUSTRIAL INFORMATICS, Deputy Editor-in-Chief of IEEE/CAA JOURNAL OF AUTOMATICA SINICA, Co-Editor of *Australian Journal of Electrical and Electronic Engineering*, an Associate Editor for 12 international journals, including theIEEE TRANSACTIONS ON CYBERNETICS, IEEE INDUSTRIAL ELECTRONICS MAGAZINE, *Control Engineering Practice, and Information Sciences*, and the Guest Editor of 14 Special Issues.